ONE STEP SYNTHESIS OF TIN-CARBON CORE-SHELL NANOPARTICLES USING LASER PYROLYSIS TECHNIQUE

Claudiu FLEACĂ[1], Florian DUMITRACHE[2], Elena DUȚU[3], Cătălin LUCULESCU[4], Ana-Maria NICULESCU[5], Alina ILIE[6], Eugeniu VASILE[7]

We report the one-step synthesis of spherical metallic tin nanoparticles having a broad diameter distribution from few nm up to 250 nm, coated with thin carbonaceous shells by using the laser pyrolysis gas-phase technique. We employed tetramethyltin as metal precursor and paraxylene as the main carbon source together with ethylene which also acts as sensitizer. After the air exposure, a superficial oxidation of the tin particles occurs due to the porosity of the carbon-based shells, as confirmed by elemental analysis and both Raman and Infrared spectra. The supplementary H_2 introduction (together with equivalent ethylene flow decreasing) or diminishing the $Sn(CH_3)_4$ flow decreases the process productivity. Moreover, the H_2 addition seems to considerably decrease the maximum nanoparticle size (down to 140 nm) and to favor the formation of the smaller ones (up to 10 nm). This kind of nanostructures have the potential to be used in high-performance anodes for lithium-ion batteries.

Keywords: Sn@C core-shell nanoparticles, laser pyrolysis, Li-ion batteries

1. Introduction

The contemporary development of the alternative energies sources designed to replace the traditional ones based on the pollutant fossil fuels is hampered by the lack of reliable and large scale energy storage systems needed to balance their variability in time. In our days, from the modern cordless electric handtools or toys to electronic mobile devices such as cellphones, tablets, laptops,

[1] Researcher, National Institute for Lasers, Plasma and Radiation Physics, Magurele and Postdoctoral Scholar, Physics Department, University POLITEHNICA of Bucharest, Romania, e-mail: claudiufleaca@yahoo.com
[2] Researcher, National Institute for Lasers, Plasma and Radiation Physics, Magurele, and Postdoctoral Scholar, Physics Department, University POLITEHNICA of Bucharest, Romania
[3] Researcher, National Institute for Lasers, Plasma and Radiation Physics, Magurele, Romania
[4] Researcher, National Institute for Lasers, Plasma and Radiation Physics, Magurele, Romania
[5] Assistant Researcher, National Institute for Lasers, Plasma and Radiation Physics, Magurele, Romania
[6] Assistant Researcher, National Institute for Lasers, Plasma and Radiation Physics, Magurele, Romania and PhD Student at Physics Faculty of Bucharest University, Bucharest, Romania
[7] Senior Researcher, Faculty of Applied Chemistry and Materials Science, University POLITEHNICA of Bucharest, Romania

as well as to electric cars, most of them are powered by lithium ion batteries who have as advantage their low production costs and relative high capacity for energy storage (due to the low atomic mass of Li element) [1]. These batteries are composed from a graphite-based anode and an oxidic cathode, sharing a common organic electrolyte and separated by a permeable membrane. When such a battery is charged, the Li^+ ions travel from cathode to anode, whereas their movement is reversed during the discharge, accompanied by an electron flow that passes through external electrical circuit. Usually, the electrolyte is composed from carbonic acid esters and lithium is introduced as $LiPF_6$ salt. However, the graphitic/carbonic anodes have a limited capacity for energy storage, requiring frequent recharges [2] due to the fact that the maximum number of Li atoms which can be intercalated in the graphite corresponds to LiC_6 with a theoretical storage capacity of 372 $mAhg^{-1}$[1] but practical around 300-310 $mAhg^{-1}$[3]. Moreover, the low density of carbon (~ $2g/cm^3$) is translated in a low volumetric capacity. Other disadvantage derives from fact that charged anode as Li_xC is a highly reducing agent. Thus, it can reduce the liquid organic electrolytes to other compounds that can have poorer Li ion conductivity [3]. The same anode has a low potential (0.1 V vs. Li) and metallic lithium can deposit as dendrites which starts from the surface of graphite at high-rate charge [3], translated in catastrophic failure of these batteries by short-circuit. In order to increase the storage performance of batteries, new anode materials were tested such as elements from the same group with carbon (Si, Sn, Ge) which can intercalate higher amount of Li and thus to store more energy per mass unit. For example, elemental tin has a theoretical maximum mass capacity of 994 $mAhg^{-1}$ or 959.5 $mAhg^{-1}$, depending of the real structure of the highest-lithiated phase $Li_{22}Sn_5$ ($Li_{4.4}Sn$) or $Li_{17}Sn_4$ ($Li_{4.25}Sn$) [4]. Moreover, the SnO_2 corresponding oxide can be also used since in contact with Li^+ ions undergoes an (partially) irreversible reduction to metallic tin which then reversibly forms the Li alloy which results in a theoretical capacity of 781 $mAhg^{-1}$ [1]. However, this advantage is accompanied by a major drawback: the great increase in volume of the Sn-Li alloy (more than 300%) due to the higher Li atomic radius (0.205 nm) compared with tin (0.172 nm) or silicon (0.146 nm) [5]. Obviously, this large volume variation during Li insertion/deinsertion is translated in mechanical tensions which pulverize the material and degrade the anode performance after only few cycles. A possibility to increase the performance of the electrode material in Li-ion battery is to use them in nanometrical form (as nanometallic particles or as nanoalloys) which can accomodate more easily large volume variations. [6]. Moreover, the use of nanomaterials have additional advantages such as those resumed in [7]:

- to significantly increase the rate of Li insertion/removal, because of the short distances for lithium-ion transport within the particles; thus the time t for

intercalation decreases with the square of the particle size on replacing micrometer with nanometer particles;

- electron transport within the particles is also enhanced by nanometer-sized particles, as described for lithium ions;
- a high surface area permits a high contact area with the electrolyte and hence a high lithium-ion flux across the interface;
- the range of composition over which solid solutions exist is often more extensive for nanoparticles and the strain associated with intercalation is often better accommodated;

One successful approach used to alleviate problems with the tin volume changes was its encapsulation inside carbon nanotubes using direct current arc discharge [8] or microwave plasmas irradiation [9] or inside carbon nanofibers as CoSn alloy [10] or carbon microtubes as Sn nanoparticles [11] using electro-spinning and thermal carbonization. Related structures consisting of Sn nanorods coated with carbon by solvothermal method showed superior reversible Li ion storage [12]. Using hydrothermal treatment of Sn acetate nanowires, the resulted mesoporous carbon nanowires containing densely encapsulated ultrafine Sn nanocrystals presented excellent electrochemical properties for Li ion batteries [13]. Other Sn/C nanostructures with spherical geometry such as the hollow shells Sn@C - Graphene hybrids [14], carbon submicron spheres filled with Sn nanoparticles (by spray pyrolysis) [15] or rambutan-like tin-carbon nanocomposites [16] show high capacity and resistance to multiple charge-discharge cycles. By combining Sn@C nanoparticles and graphenes in 3D network using hydrothermal approach, high-performance porous electrode materials for Li batteries were obtained [17], [18]. Other special geometry that enhances the Li-ion battery anode performances was obtained by encapsulating Sn nanoparticles into elastic hollow carbon spheres [19].

Usually, the methods used for the synthesis of Sn-C nanostructures require multiple laborious steps to achieve such special architectures, which are costly and time-consuming. A promising technique for single-step synthesis of Sn@C nanoparticles is the laser pyrolysis. Our team recently reported the obtaining of Sn and SnFe nanoparticles (with carbon content) by this method starting from tetramethyltin precursor and ethylene sensitizer [20], [21]. In this work, starting from the same sensitizer and Sn precursor we report the successful laser pyrolysis synthesis of tin nanoparticles coated with carbonaceous layer by adding paraxylene vapors (as supplementary carbon donor) and their characterization.

2. Methods and materials

For the laser pyrolysis experiments, we used tetramethyltin (99.99%, from Merk) and paraxylene (99%, from Reactivul) volatile liquids, as

well as gaseous C_2H_4 (99.95%), H_2 (99.99%) and Ar (99.99%) from Linde Gas. The reaction flame temperature was monitored using an IRtec P2000 Optical Pyrometer and the Laser power with a LM-200 HTD Powermeter. The obtained samples have been characterized PANalytical X'Pert PRO MPD X-ray diffractometer using Cu X-ray tube providing the K wavelength of 1.5418 Å and the resulted diffractograms were analyzed with the PANalytical X'Pert High-Score Plus software package. Energy-dispersive X-ray spectroscopy (EDX) measurements for elemental analysis were performed inside a scanning electron microscope (SEM) FEI Quanta Inspect S, 0–30 kV accelerating voltage, using an EDAX Co. liquid nitrogen cooled SiLi detector and few tens of mg of nanopowder pressed with the aid of an aluminium foil on a pure nickel substrate. The same microscope was used for aquiring the SEM images. We employed a Tecnai F30 G2 (300 kV) transmission electron microscope (TEM) for the obtaining of transmission electron microscopy images at low or high resolution. The Raman spectra were acquired using a MicroRaman Spectrometer Jasco NRS 7200 using a 532 nm wavelength green laser.

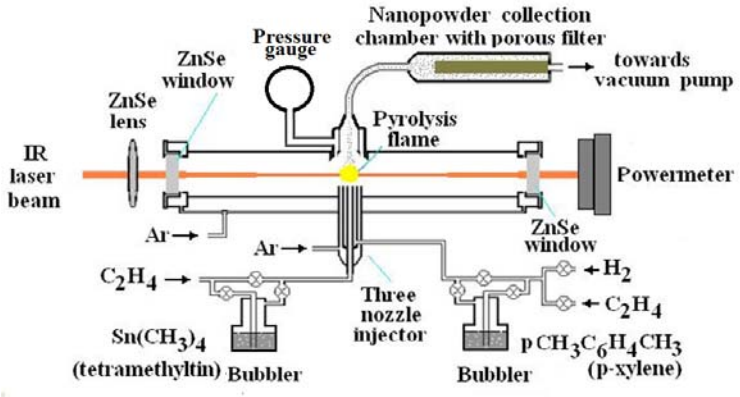

Fig. 1. Experimental set-up for the laser pyrolysis synthesis of Sn@C nanoparticles

Laser pyrolysis method is based on the absorption of the CO_2 laser infrared photons (λ = 10.6μm) by the sensitizer molecules, their vibrational/ rotational excitation and decomposition which is accompanied by collisions with other non-absorbing species. As a result, the gas/vapor mixture is heated very fast, resulting reactive atoms and radicals which subsequently will interact to produce nanoparticles which leave the reactive zone.

In our case we employed a Coherent Diamond CO_2 pulsed laser (frequency 200 kHz, duty factor 50%) whose emitted beam orthogonally intersects the reactive flows provided by the three concentric nozzles injector as depicted in Fig.1. The main parameters of the laser pyrolysis experiments are summarized in Table 1.

Table 1

Main experimental parameters of the Sn@C nanoparticles synthesis

Experiment	**Central (inner) flow** $D_{C2H4/Sn(Me)4}$ [sccm]	**Intermediate flow** $D_{C2H4/p\text{-}xylene}$ [sccm]	$D_{H2/p\text{-}xylene}$ [sccm]	**Outer flow** $D_{Ar\ conf}$ [sccm]	Laser power $_{under\ Ar/\ after\ absorption}$ [W]	Flame temperature [°C]	Powder Productivity [g/h]
SPP1	5	130	0	2500	70/66	620	0.30
SPP2	5	100	30	2500	70/67	600	0.25
SPP3	3	130	0	2500	70/67	580	0.14

$D_{Ar\ Windows}$ = 2 x 150 sccm; Working pressure = 450 mbar (45000Pa)
$\Phi_{inner\ nozzle}$ = 0.9 $_{mm}$; $\Phi_{middle\ nozzle}$ = 2.3 mm; $\Phi_{outer\ nozzle}$ = 14 mm

The three experiments employed the same p-xylene vapor flow through the second annular nozzle, with the partial replacement of C_2H_4 carrier gas by H_2 in SPP2 experiment. The tin precursor flow (also carried by ethylene sensitizer) through the inner nozzle was kept constant for SPP1 and SPP2 experiments and was diminished for the third one (SPP3).

3. Results and discussions

The proposed formation mechanism for the tin core-carbonaceous shell nanoparticles in our experimental conditions is presented in Fig.2. Due to the intense laser energy absorption by the ethylene molecules, the reactive mixture is heated very fast around 600°C (see Table 1), starting the dehydrogenation reaction of p-xylene with the formation of p-methylbenzyl radical, similar with those reported in [22] for the paraxylene pyrolysis in inert atmosphere. This radical also undergoes dehydrogenation with 61.5 kcal.mol dissociation energy, resulting paraxylilene diradical (who have also a paraquinoid mesomeric structure) [23]. This intermediate can also undergo cyclization or polymerization with the formation of parylene oligomers [24], but in our laser pyrolysis conditions the possible reactions are much more complicated due to the presence of methyl (from $Sn(CH_3)_4$ decomposition) and ethyl (from C_2H_4) free radicals. Another important factor is the presence of tin atoms and clusters provided also by the tetramethyltin molecules, Their decomposition in presence of toluene was studied between 803 and 941 K at lower pressures and implies both sequential demethylation and subsequent reactions of methyl radicals, with an extracted $D[(CH_3)_3Sn\text{-}CH_3]$ 64.5 kcal/mol tin-carbon dissociation energy from Arrhenius plot [25]. Due to the low melting point of bulk tin (506 K), in our conditions (with the flame temperature over 850 K) the tin particles are in liquid phase (as nanodroplets). We assume that the polymers and macroradicals can be adsorbed on the Sn particles surface and undergo subsequent reticulation /dehydrogenation reactions with formation of a porous carbonaceous shell.

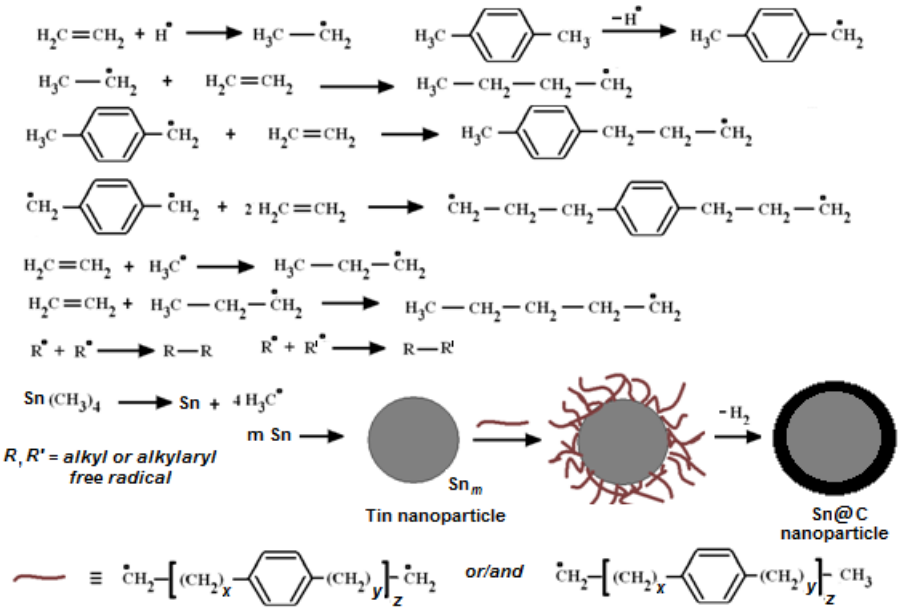

Fig.2 Proposed mechanism for the formation of Sn@C nanoparticles in our experiments

Due to the very low carbon solubility in melted tin (0.002 at. % at temperatures higher than 1800 K [26]), no tin carbide phases or solutions can be formed and the carbon-based material is accumulating on the tin nanodroplets surface.

Very little differences (2-3%, in the range of the experimental errors) in the elemental compositions estimated from EDX analyses (mediated from two measurements on different zones using 15 keV acceleration voltage of filament-emitted electrons from each nanopowder) were found between the three samples: ~ 60% at.% Sn, ~ 23 at.% C and ~ 17% C, in spite of different amount of carbon and tin precursors introduced in the reactive zone. Yet, for the SnC3 experiment, where the lowest quantity of tin was introduced (as $Sn(CH_3)_4$ via ethylene bubbling), the powder productivity was considerably lower than in the first two experiments (see Table 1). Thus, it seems that the Sn/C atomic ratio in the resulted nanopowders is quite insensitive to the same ratio extracted from the amount of the introduced precursors ($Sn(CH_3)_4$, C_2H_4 and $CH_3C_6H_4CH_3$). Being obtained in an anoxic environment, the considerable amount of oxygen found in all three samples can be explained only by the post-synthesis air exposure of nanopowders. This means that the porous carbonaceous layer allows the oxygen permeation, thus a superficial oxidation occurs on tin nanoparticles. Also, a certain amount of oxygen can be bound to carbon (resulting oxygenated functions such as carboxyl, carbonyl, lactone etc) after ambient atmosphere exposure due to the existence of reactive dangling bonds from the unreacted free radicals attached to the

carbonaceous layer. Even if the tin oxide phases are not visible in X-ray diffractograms (where only the beta tin metallic phase peaks appear - see Fig.3 left column), their presence in the Raman spectra is obvious (see 250-750 cm^{-1} zone from Fig.3 right column).

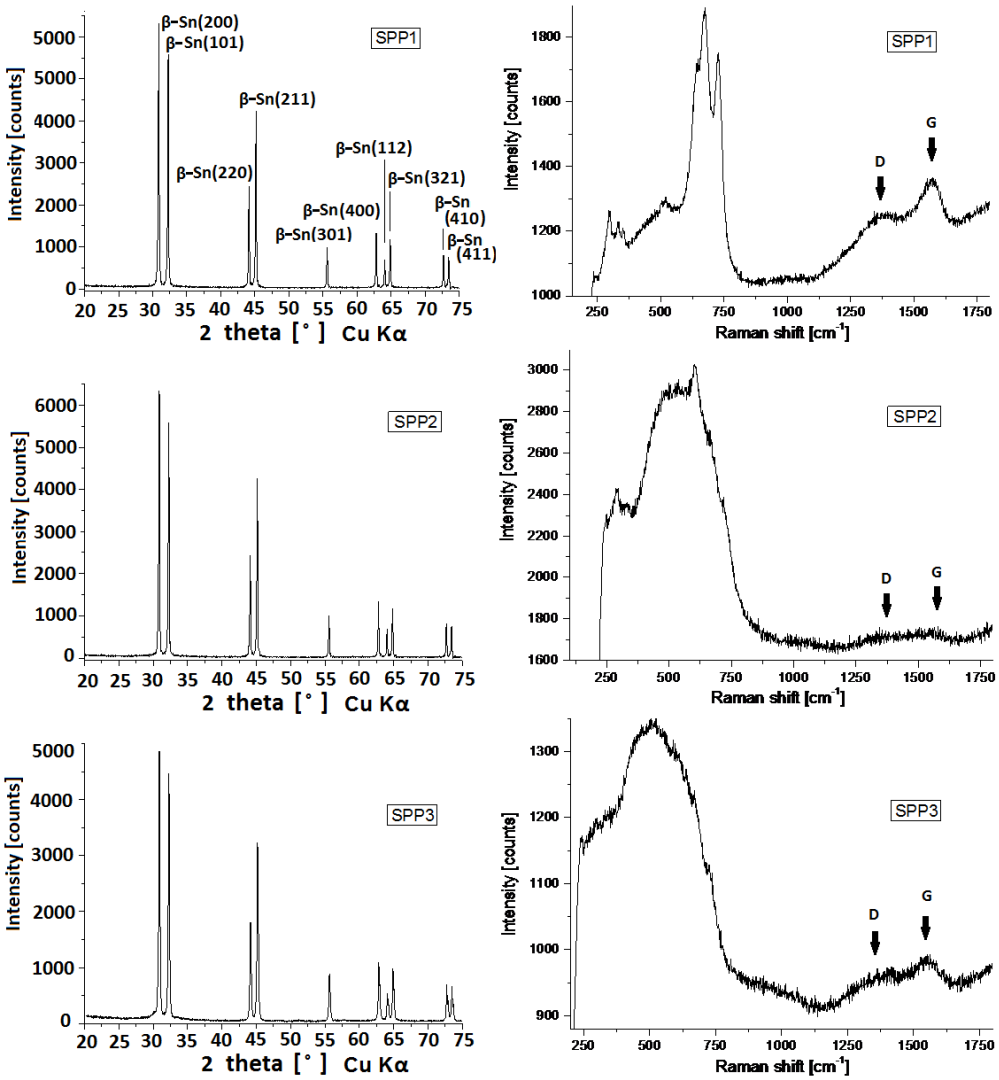

Fig. 3. Superposed X-ray diffractograms (left column) and Raman spectra (right column) from the SPP1, SPP2 and SPP3 tin-based nanopowders

The intensity of tin oxide bands from Raman spectra seems to be enhanced under the heating effect of the green laser of Raman apparatus in the presence of

environmental air. For the chemically synthesized SnO_2 nanocrystals the most intense reported Raman peak was attributed to A_{1g} vibration mode at 630 cm^{-1} [27]. For SPP1 sample, the nearest peaks were found at 648 and 675 cm^{-1}, whereas for SPP2 sample at 602 cm^{-1}. The presence of a broad peak, between 400 and 800 cm^{-1} was reported in the Raman spectrum of $Ag/Ag_xSn/SnO_2$ type nanocomposites [28], where the authors identified three convoluted peaks of tin dioxide: E_g at 472 cm^{-1}, A_{1g} at 633 cm^{-1} and B_{2g} la 775 cm^{-1}. These three principal Raman peaks were established in [29]. Contributions of nanometric and amorphous SnO_2 were also observed at 523 and 625 cm^{-1} (as shoulder), respectively [28]. In our samples, the most intense Raman peaks can be found at 675 cm^{-1} for SPP1 and 690 cm^{-1} for SPP2 (see Fig.2, right column). The latest is near to the 708 cm^{-1} peak, tentatively attributed to B_{2g} mode in undoped tin dioxide [27]. The position variation of the three main Raman peaks of nanometric SnO_2 was also reflected in [30] where the following values were reported: 475 cm^{-1} (E_{2g}, very weak), 658.9 cm^{-1} (A_{1g}) and 750 (B_{2g}) for oxygen- deficient tin dioxide nanostructures. Also, in the same reference [30], the authors believe that the nanometric dimension allows the emergence of some forbidden vibrational modes in bulk crystals). Such peak - attributed to longitudinal optical phonons - is considered those from 694.1 cm^{-1} who doesn't exists in bulk tin dioxide with rutile structure. The presence of broad, convoluted D (around 1360-1380 cm^{-1}) and G (around 1600 cm^{-1}) bands attributed to defected and crystalline graphite, respectively can be seen in all three nanocomposites (Fig.3, right column). The most intense Raman G peak - and thus the best graphitization from the three nanopowders - comes from the SPP1 sample synthesized with the highest ethylene flow at the higher temperature (see table 1), having also the highest carbon and lowest oxygen content (see Table 2) which reflect a lower porosity. The Raman spectra reported in [28] contains notonly the tin dioxide but also the carbon Raman signature, being similar with our carbon spectra from SPP1 and SPP3 samples. In their synthesis, the carbon is provided by (fluorinated)acetylacetonate ligands from organometallic precursors decomposition. They find the more intense G band at 1597 cm^{-1} and a weaker, shoulder-like D band at 1274 cm^{-1}. Moreover, they report the presence of a third weak peak (also like a shoulder) situated between D and G bands at 1490 cm^{-1}, attributed to hydrogenated amorphous carbon. This peak can be extracted also from our Raman spectra upon deconvolution of carbon bands zone and can be a result of a partial dehydrogenation of the reticulated polymers around Sn nanoparticles. Finally, the presence of H_2 in the reaction mixture (SPP2 experiment) seems to provide a very poor graphitization, reflected in a very weak and broad G peak.

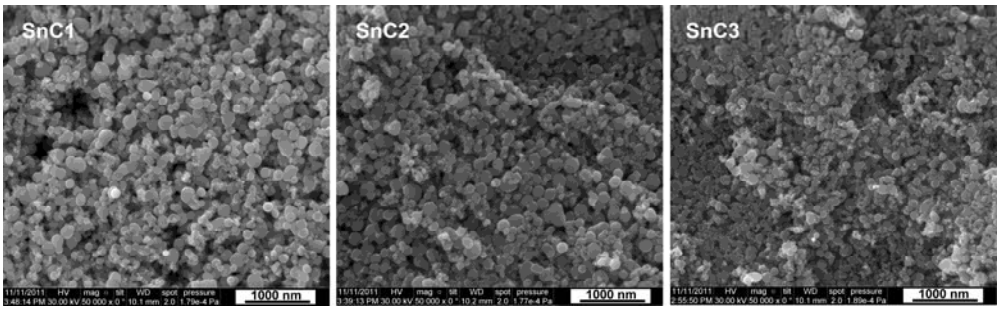

Fig. 4 SEM images from the three nanopowders

All the SEM images of the three tin-based powders from Fig.4 show a mixture of smaller and bigger spheroidal particles with relative high packing density. The high resolution TEM images from the left part of Fig, 5 and 6 confirm the presence of crystalline metallic β-Sn: Sn(200) at 2.92 Å and Sn(220) at 2.10 Å whose X-ray diffraction peaks were presented in the left column of the Fig.2. The main crystallite size extracted from XRD (211) peak was 57.1 nm for SPP1 and 59.8 nm for SPP2. The TEM images reveal a broad distribution of nanoparticles diameter, from those very small (around 10 nm or less) up to those over 100 nm. As can be seen in the Fig. 5, particles with similar sizes appear to be bounded together as chains, a sign that they nucleate and then coalesce before solidification in a confined volume.

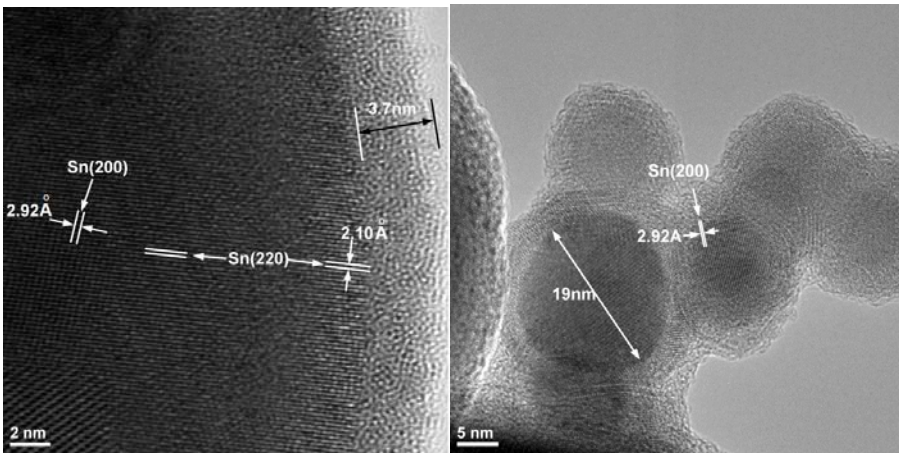

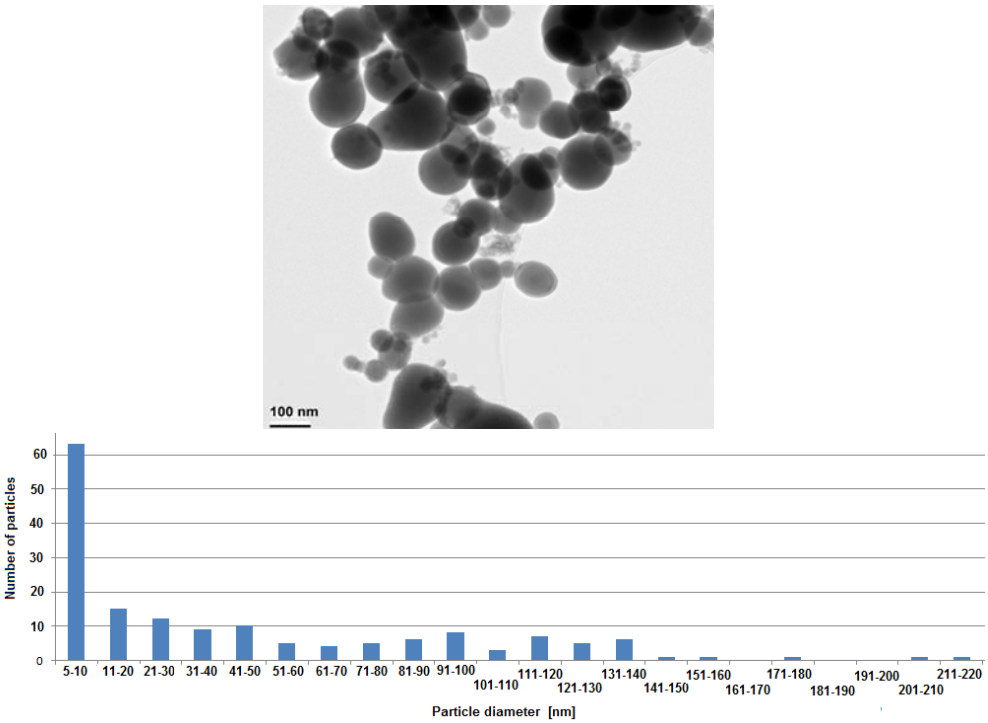

Fig. 5 High (up) and low (down) resolution TEM images of nanoparticles from SPP1 nanopowder together with the particle size distribution hystogram extracted from lower TEM image

The welding of the particles can be explained by the collision of two partially solidified nanoparticles that can't merge to form a bigger round nanoparticle. We suppose that the coalescence of small Sn nanodroplets is very fast, in some conditions this process being stopped once they are covered with a carbonaceous layer, even if the tin core is still liquid. The presence of few nm disordered layer around each spherical tin-based particle is clearly visible in all high resolution TEM images. Corroborating these images data from with EDX-extracted elemental composition and X-ray diffractograms information, one can deduce that this shell is composed from carbonaceous substance and (as can be seen from the left image of the Fig.7 where a thicker layer is visible) from the left image of the Fig.6 where a thicker layer is visible) from disordered SnO_x formed by oxygen diffusion through the porous external layer after exposure to ambient air. The quasispherical shape of our nanoparticles can be explained by their transient liquid state when they are suspended in the hot gaseous medium, where the superficial tension of liquid tin imposes a minimization of their free surface. Yet, the simultaneous presence in all of the three samples of nanoparticles with very different sizes suggests that the coalescence is blocked only for certain small

nanoparticles, whereas others undergo coalescence with formation of bigger particles, in spite of the apparent solid carbonaceous wall presence.

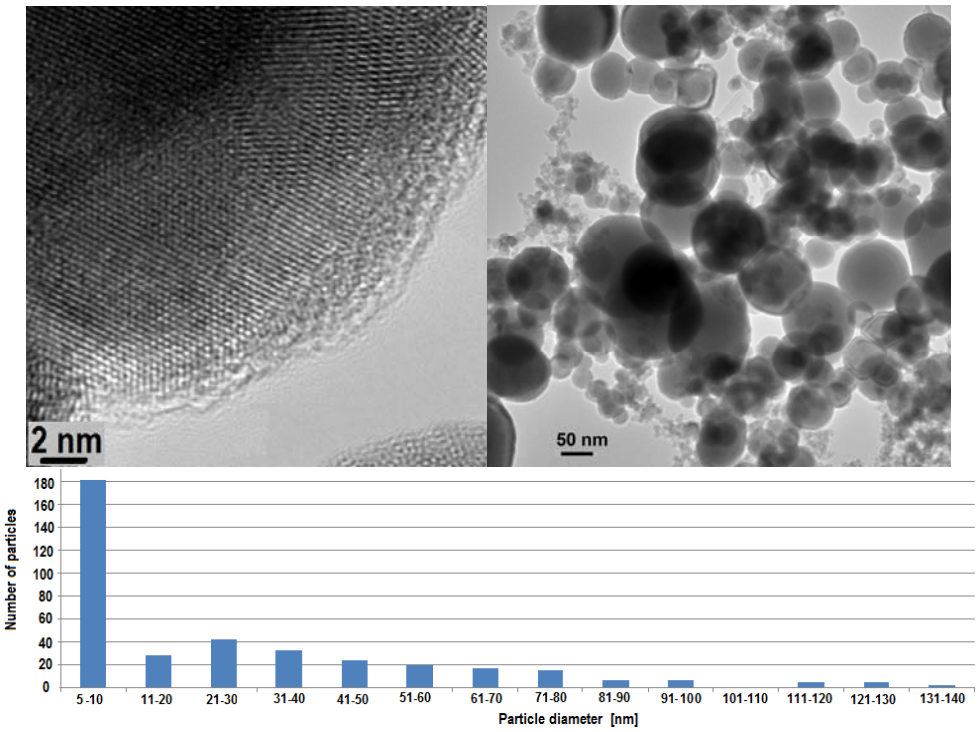

Fig. 6 High (left) and low (right) resolution TEM images of nanoparticles from SPP2 nanopowder and the corresponding particle size

One tentative explanation can be that in some cases, in the hot reaction zone, the very flexible thin carbonaceous layer can allow the liquid-liquid contact through pores or through a mechanism including some kind of openings formation followed by rearrangement, somehow similar with the fusion of two surfactant-covered liquid aqueous vesicles. Also, the local conditions from the laser-assisted pyrolitic flame may play a role in the formation of particles with very different sizes – on the central zone, there is a low concentration of carbon precursors (tetramenthytin and ethylene), whereas on the concentric surrounded flow there is a higher concentration of carbon precursors (xylene vapors and ethylene) – see Table 1. This fact implies the formation first of a very thin carbonaceous layer in the central zone where the $Sn(CH_3)_4$ molecules decomposes, followed by coalescence and then by the growth of a thicker carbon layer from xylene polymerization /dehydrogenation/decomposition also in the presenceof ethylene molecules. Other observation concerns the narrowing of the size distribution of

nanoparticles accompanied by the enhancing of the small nanoparticles (under 10 nm) production resulted from SnC2 experiment when compared with those from SnC1 and SnC3 runs. The near 100 nm decrease of the maximum size of the nanoparticles resulted in that experimentand the enhancement of number of the coalescence-avoided small nanoparticles can be related to the hydrogen introduction and/or to the corresponding ethylene decreasing which can influence the xylene molecules dehydrogenation and their susbsequent decomposition.

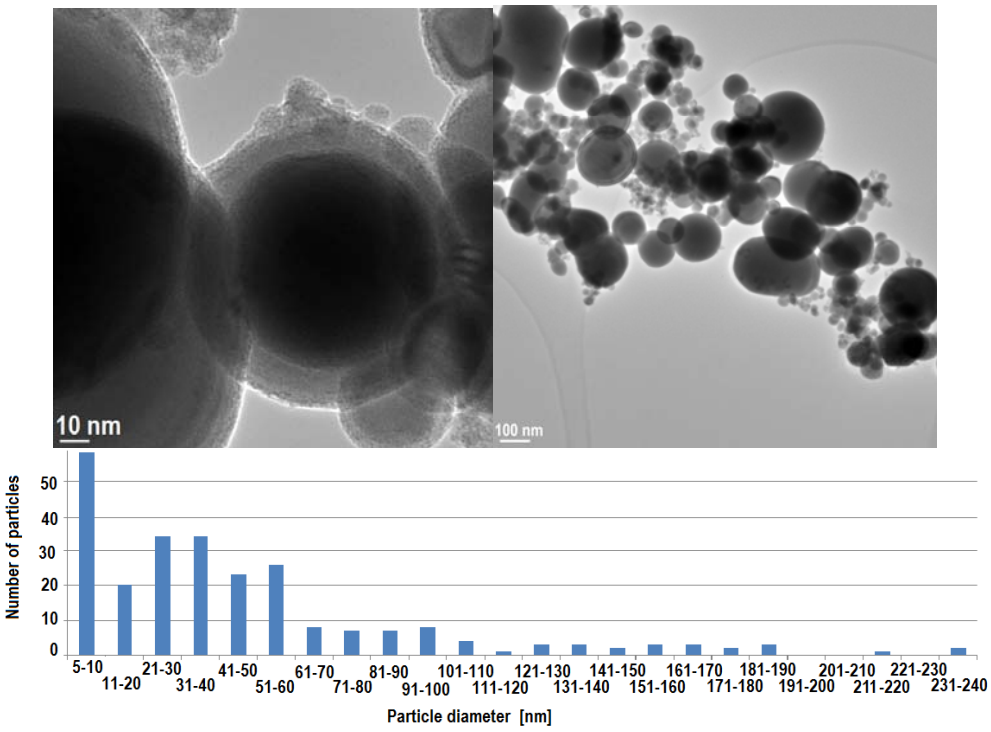

Fig. 7 High (left) and low (right) resolution TEM images of nanoparticles from SPP3 nanopowder and the corresponding particle size distribution

4. Conclusions

Using laser pyrolysis technique and a three concerntric nozzles configuration we synthesized Sn@C nanocomposites starting from $Sn(CH_3)_4$ and p-$CH_3C_6H_4CH_3$ precursors in the presence of C_2H_4 laser energy transfer agent. The core of nanoparticles contains metallic tin, whereas the shell seems to be a mixture of disordered carbon and non-crystalline tin oxides. The introduction of H_2 (partially replacing C_2H_4 as p-xylene carrier) increases the number of small nanoparticles, decreasing the maximum diameter of bigger ones. Due to their

special configuration and nanometric size, this kind of tin nanocomposites could be applied in the construction of advanced anodes for Li-ion batteries.

Acknowledgements

The work has been funded by the Sectoral Operational Programme Human Resources Development 2007-2013 of the Ministry of European Funds through the Financial Agreement POSDRU/159/1.5/S/132395 and by Nucleu Program PN 09 39 and PN-II-RU-TE-2014-4-2834 Program financed by the Romanian Ministry of National Education.

R E F E R E N C E S

[1] *J. Chen*, "Recent Progress in Advanced Materials for Lithium Ion Batteries", in Materials **vol.6**, 2013, pp. 156-183.

[2] *M.M. Thackeray, C.Wolverton, E.D. Isaacs*, "Electrical energy storage for transportation—approaching the limits of, and going beyond, lithium-ion batteries", in Energy Environ. Sci. **vol.5**, no.7, 2012, pp. 7854-7863.

[3] *B.W.R. Chowdari*, "Bulk- and nanomaterials for Li ion batteries" in http://www.rakcam.org /Files/B.V.R.Chowdari - Bulk- and Nano Materials as Electrodes for Li Ion Batteries.pdf.

[4] *G.R. Goward, N.J. Taylor, D.C.S. Souza, L.F. Nazar*, "The true crystal structure of $Li_{17}M_4$ (M = Ge, Sn, Pb) – revised from $Li_{22}M_5$", in J. Alloys Cpds. **vol.329**, no.1-2, 2001, pp. 82-91.

[5] *D. Larcher, S. Beattie, M. Morcrette, K. Edstrom, J.-C. Jumas, J.-M.Tarascon,* "Recent findings and prospects in the field of pure metals as negative electrodes for Li-ion batteries" in J. Mater. Chem. **vol.17**, no.36, 2007, pp. 3759–3772.

[6] *M. Winter, J.O. Besenhard,* " Electrochemical lithiation of tin and tin-based intermetallics and composites" in Electrochimica Acta **vol.45**, no.1-2 , 1999, pp. 31–50.

[7] *P. G. Bruce, B. Scrosati, J.-M. Tarascon*, "Nanomaterials for Rechargeable Lithium Batteries" in Angew. Chem. Int. Ed. **vol.47**, no.16 , 2008, pp. 2930 – 2946.

[8] *C. Liu, H. Huang, G. Cao, F. Xue, R.A. Paredes Camacho, X. Dong*, "Enhanced electro-chemical stability of Sn-Carbon nanotube nanocapsules as Lithium-ion battery anode" in Electrochimica Acta **vol.144**, 2014, pp. 376–382.

[9] *N. Li, H. Song, H. Cui,G. Yang, C. Wang,* "Self-assembled growth of Sn@CNT on vertically aligned graphene for binder-free Li-storage and excellent stability" in J. Mater. Chem. A **vol.2**, no.8, 2014, pp. 2526-2537.

[10] *W. Lu, C. Luo, Y. Li, Y. Feng, W. Feng, Y. Zhao, X. Yuan,* "CoSn/carbon composite nanofibers for applications as anode in lithium-ion batteries", in J. Nanopart. Res. **vol.15**, no. 9, 2013, pp.1736-1746.

[11] *I. Meschini, F. Nobili, M. Mancini, R. Marassi, R. Tossici, A. Savoini, M. L. Focarete, F. Croce,* "High-performance Sn@carbon nanocomposite anode for lithium batteries" in J. Power Sources **vol.226**, no. 15, 2013, pp. 241-248.

[12] *P. Wu, N. Du, J. Liu, H. Zhang, J. Yu, D. Yang*, "Solvothermal synthesis of carbon-coated tin nanorods for superior reversible lithium ion storage" in Mater. Res. Bull. **vol.46**, no. 12, 2011, pp. 2278–2282.

[13] *Y. Qiu, K. Yan, S.Yang,* "Ultrafine tin nanocrystallites encapsulated in mesoporous carbon nanowires: scalable synthesis and excellent electrochemical properties for rechargeable lithium ion batteries" in Chem. Commun. **vol.46**, no. 44, 2010, pp. 8359–8361.

[14] *X. Zheng, W. Lv, Y.-B. He, C. Zhang, W. Wei, Y. Tao, B. Li, Q.-Hong Yang*, "3D Hollow Sn@Carbon-graphene hybrid material as promising anode for Lithium-ion batteries" in J. of Nanomaterials, **vol. 2014**, Art. ID 974285, 6 pag..

[15] *Y. Xu, Q. Liu, Y. Zhu, Y. Liu, A. Langrock, M.R. Zachariah, C. Wang,* "Uniform nano-Sn/C composite anodes for Lithium ion batteries" in Nanoletters **vol.13**, no. 2, 2013, pp.470-474.

[16] *D. Deng, J.Y. Lee,* "Reversible storage of Lithium in a rambutan-like Tin–Carbon electrode" in Angew. Chem. Int. Ed. **vol.48**, no. 9, 2009, pp. 1660 –1663.

[17] *P. Lian, J. Wang, D. Cai, G. Liu, Y. Wang, H. Wang*, "Design and synthesis of porous nano-sized Sn@C/graphene electrode material with 3D carbon network for high-performance lithium-ion batteries" in J. Alloys Compounds **vol.604**, 2014, pp.188–195.

[18] *S. Liang, X. Zhu, P. Lian, W. Yang, H. Wang*, "Superior cycle performance of Sn@C/ graphene nanocomposite as an anode material for lithium-ion batteries" in J. Solid State Chem. **vol.184**, no. 6 ,2011, pp. 1400–1404.

[19] *W.-M. Zhang, J.-S. Hu, Y.-G. Guo, S.-F. Zheng, L.-S. Zhong, W.-G. Song, L.-J. Wan,* "Tin-nanoparticles encapsulated in elastic hollow carbon spheres for high-performance anode material in Lithium-ion batteries" in Adv. Mater. **vol.20**, no.6, 2008, pp. 1160–1165.

[20] *R. Alexandrescu, I. Morjan, F. Dumitrache, Birjega, C. Fleaca, I. S. Morjan, M. Scarisoreanu, C.R. Luculescu, E. Dutu, V. Kuncser, G. Filoti, E. Vasile, V. Ciupina* "Laser processing issues of nanosized intermetallic Fe-Sn and metallic Sn particles" in Appl. Surf. Sci. **vol.258** , no. 23, 2012, pp.9421-9426.

[21] *E. Dutu, F. Dumitrache, C. T. Fleaca, I. Morjan, L. Gavrila-Florescu, I.P. Morjan, I. Sandu, M. Scarisoreanu, C. Luculescu, A.- M. Niculescu, E. Vasile* , "Metallic tin-based nanoparticles synthesis by laser pyrolysis: parametric studies focused on the decreasing of the crystallite size" in Appl. Surf. Sci. **vol.336**, 2015, pp. 290-296.

[22] *L.V. Shevelkova, V.G. Sokolovskaya, L.Y. Guselnikov, V.N. Guryshev,* "Mechanism of pyrolysis of *p*-xylene " in Petroleum Chem. USSR **vol. 29**, no. 2, 1989, pp. 114-123.

[23] *G. da Silva, E.E. Moore, J.W. Bozzelli* , "Decomposition of methylbenzyl radicals in the pyrolysis and oxidation of xylenes" in J. Phys. Chem. A **vol.113**, no. 38, 2009, pp. 10264-10278.

[24] *A. Kumar, A. N. Rao, S. K. Gupta,* "Quenching of pyrolysis products of p-xylene in toluene- a kinetic studies of acetone-soluble products" in Canadian J. Chem Eng **vol.57**, no. 3, 1979, pp. 304-310 .

[25] *R. P. Johnson, S. J. W. Price,* "The Pyrolysis of Tetramethyltin" in Canadian J. Chem. **vol.50**, no. 1, 1972, pp. 50-54.

[25] *L. L. Oden N. A. Gokcen, "*Sn-C and Al-Sn-C phase diagrams and thermodynamic properties of C in the alloys: 1550 °C to 2300 °C" in Metallurgical Transactions B **vol.24**, no. 1, 1993, pp 53-58.

[27] *J. Kaur, R.K. Kontala, K.C. Verma, "*Raman spectra and ferromagnetism of pure, Co and Fe doped SnO_2 nanoparticles*"* in Ceramics Int. **vol.38**, no. 7, 2012, pp. 5563-5570

[28] *T. Křenek, P. Duchek, M. Urbanová, D. Pokorná, P. Bezdička, I. Jakubec, M. Pola, R. Čerstvý, T. Kovářík, A. Galiková, J. Pola, "*Thermal co-decomposition of silver acetylacetonate and tin(II) hexafluoroacetylacetonate: Formation of carbonaceous Ag/Ag_xSn ($x = 4$ and 6.7)/SnO_2 composites*"* in Thermochim. Acta **vol.566** , 2013, pp. 92-99.

[29] *P.S. Percy, B. Morosin, "*Pressure and temperature dependence of the Raman-active phonons in SnO_2*"*, in Phys. Rev. B **vol.7**, no. 6, 1973, pp. 2779-2786.

[30] *Q.-H. Wu, J. Song, J. Li, "*High oxygen vacancy tin oxide synthesized by combustion chemical vapor deposition (CCVD)*"* in Surface Interface Analysis **vol.40**, no. 11, 2008, pp.1488-1469.